SeRadar: Embracing Secondary Reflections for Human Sensing with mmWave Radar

Danei Gong[‡], Naiyu Zheng[‡], Binbin Xie[§], Jie Xiong[†], Shuai Wang[¶], Yuguang Fang[‡], Zhimeng Yin[‡*]

[‡]City University of Hong Kong [§]University of Texas at Arlington
[†]Nanyang Technological University [¶]Southeast University

ABSTRACT

Millimeter-wave (mmWave) has emerged as a promising solution for contact-free sensing due to its high resolution. Although promising, it faces several critical issues, including occlusion from the surrounding environment, unstable orientation-dependent sensing performance, and significant interference when multiple targets are in close proximity. These fundamental issues hinder the widespread adoption of mmWave sensing in the real world. In this paper, we propose SeRadar, the first systematic framework that leverages all useful secondary reflections to significantly enhance reliability and bring mmWave sensing one step closer to real-world adoption. Unlike primary reflections commonly used in wireless sensing, secondary reflections—typically much weaker due to being reflected multiple times—are generally ignored in existing literature. However, we observe that secondary reflections are common in various scenarios and carry valuable information about target movements, which could also contribute to sensing. To effectively utilize secondary reflections for sensing, SeRadar addresses several challenges associated with secondary reflections. Specifically, it boosts weak secondary reflections to improve their sensing capability, identifies useful ones from a large number of secondary reflections captured in the environment, and mitigates primary-secondary interference in multi-target scenarios. We evaluate the performance of SeRadar in various environments, including offices, apartments, and vehicle cabins. Extensive experiments demonstrate SeRadar can enhance accuracy and reliability in diverse sensing scenarios.

*Zhimeng Yin is the corresponding author

ACM MOBICOM '25, November 4–8, 2025, Hong Kong, China

ACM ISBN 979-8-4007-1129-9/2025/11
https://doi.org/10.1145/3680207.3723471

CCS CONCEPTS

• **Human-centered computing → Ubiquitous and mobile computing systems and tools**.

KEYWORDS

Wireless sensing, MmWave Radar, Secondary reflections

ACM Reference Format:
Danei Gong[‡], Naiyu Zheng[‡], Binbin Xie[§], Jie Xiong[†], Shuai Wang[¶], Yuguang Fang[‡], Zhimeng Yin[‡]. 2025. SeRadar: Embracing Secondary Reflections for Human Sensing with mmWave Radar. In *The 31st Annual International Conference on Mobile Computing and Networking (ACM MOBICOM '25), November 4–8, 2025, Hong Kong, China.* ACM, New York, NY, USA, 16 pages. https://doi.org/10.1145/3680207.3723471

1 INTRODUCTION

In recent years, significant efforts have been devoted to utilizing wireless signals for pervasive intelligent sensing. The basic rationale behind wireless sensing is that wireless signals reflected from targets vary with target motions. Through analyzing the induced signal variations (e.g., amplitude and phase changes), target motions can be inferred. A large range of applications have been realized with wireless sensing including gesture/activity recognition [25, 28, 72], intrusion detection [21, 38, 69], vital sign monitoring [9, 13, 55], and even target size and material sensing [35, 45, 50]. Various wireless signals have been utilized for sensing including WiFi [46, 59, 73], LoRa [19, 51, 52], sound [3, 47, 68], RFID [8, 45, 53], and mmWave [43, 57, 66]. Among the signals exploited for sensing, mmWave stands out owing to its large frequency bandwidth and accordingly high resolution in terms of sensing granularity. It has been widely used for sensing fine-grained human activities such as gestures [24].

While promising, there are still issues associated with mmWave-based sensing. (i) The high carrier frequency is a double-edged sword. While it brings high range resolution due to broad bandwidth, the penetration capability of mmWave is low, meaning mmWave signals can be easily occluded by objects in the environment (Fig. 1a). (ii) The sensing performance is highly orientation-dependent. Take gesture recognition as an example, the signal features can be very different when the human target is facing different orientations (Fig. 1b). This causes high recognition errors

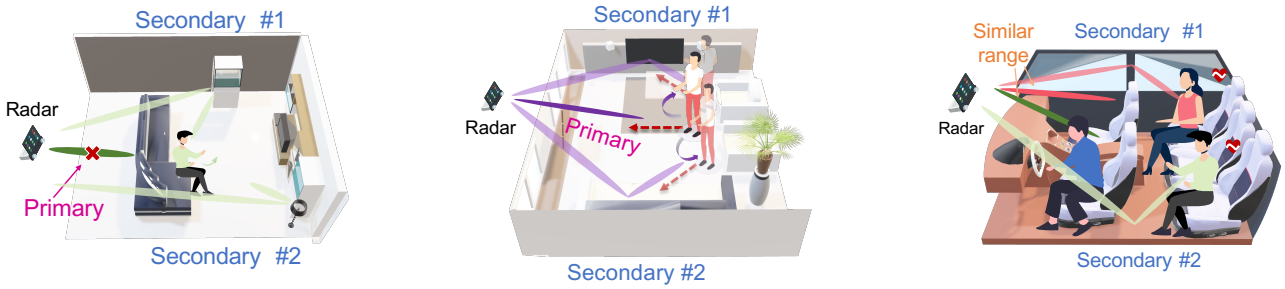

(a) Indoor sensing when the target is occluded by a sofa.

(b) Sensing the target with orientation change.

(c) Sensing multiple targets inside a vehicle cabin.

Figure 1: Scenarios of wireless sensing failure utilizing the primary reflection in reality.

and what is worse, low generalizability because the same gesture can cause dramatically different signal features. (iii) Although mmWave radars achieve a high range resolution, it is still challenging when multiple sensing targets are within a small space, such as car cabins (Fig. 1c), where signals from multiple targets can be mixed in the same range bin.

In this paper, we propose to exploit the *secondary reflections*, traditionally ignored in wireless sensing to address all the issues above, moving mmWave sensing one step towards real-life adoption. Our idea is inspired by the fact that existing mmWave sensing systems always rely on the primary reflection, which is reflected by the target and reaches the receiver without other intermediate reflections, usually exhibiting the strongest signal strength. However, we observe that *the secondary reflections (i.e., signals reflected once at the target and once at another object in the environment such as furniture or wall) widely exist, which also contain useful target information.* Although they are weaker than the primary reflection, they can still be utilized for sensing in a lot of scenarios. What is more important, different from narrowband signals such as WiFi, the primary and secondary reflections of mmWave signals are inherently separated in different range bins. Employing secondary reflections for sensing presents us with the following benefits.

- Blind spot is a severe issue in wireless sensing [7]. When primary reflection is occluded, we can still employ secondary reflections for sensing, mitigating this issue.
- Secondary reflections present multiple "sensing views" from different angles compared to the primary reflection. This helps address the orientation-dependent issue in wireless sensing. With secondary reflections, we do not require the target to face a particular orientation and the diverse sensing features extracted at different views greatly enhance the generalizability of RF sensing.
- Secondary reflection helps address the multi-target sensing problem, one well-known challenge in wireless sensing. Even the primary reflections are close to each other, the secondary reflections can be much further away due to distinct propagation paths and reflection surfaces, resulting in different arrival angles and time delays at the receiver to enable multi-target sensing.

Inspired by the above observations, we propose **SeRadar**, a system that exploits secondary reflections to significantly enhance the sensing performance. While it is a promising technique, several challenges need to be tackled before we can turn the idea into a functional system.

- While secondary reflections contain the target information, they are much weaker than the primary reflections and thus critical signal features for sensing can be buried in the noise. It is challenging to effectively utilize secondary reflections for fine-grained sensing.
- There are usually a large number of secondary reflections in the environment and not all of them are reflected from the region of interests (ROI) of the target. It is non-trivial to identify those "useful" secondary reflections for sensing.
- When there is only one target, the primary reflections and secondary reflections are usually separated into different range bins. However, when multiple targets exist, the problem becomes more challenging because the primary reflection of one target can be in the same range bin as the other target's primary or secondary reflection.

To address the first challenge, we propose to strengthen weak secondary reflections to improve sensing capability. Our intuition is that the size of reflectors in the environment is typically much larger than the range resolution of the mmWave radar. In this case, signals can be reflected from multiple points at the reflector. Benefiting from mmWave signal's large bandwidth, these reflections fall into multiple adjacent range bins, each exhibiting independent noise characteristics. We thus propose to aggregate these signals to enhance secondary reflections for sensing. For the second challenge, we leverage an interesting observation that among the large number of secondary reflections, those with target information are correlated. We thus apply the mutual information coefficient (MIC) metric [20] to measure the possibility of signals containing similar target information and accordingly identify those useful secondary reflections without requiring any pre-measured pattern or feature. To address the challenge of separating signals reflected from multiple targets, we formulate the problem as an optimization task. The objective is to search for the steering vectors

that maximize the signal strength at the target angle of interest while simultaneously minimizing the signal strengths at the angles of other targets. Note that the inherent large bandwidth of mmWave and beamforming technique help separate signals in the time domain and the spatial domain respectively. With these two orthogonal separations, the interference between signals is dramatically reduced.

We implemented SeRadar using commercial millimeter-wave hardware and conducted comprehensive experiments in several representative environments including office, home, and car cabin. We employed gesture recognition (macro-motion sensing) and breath monitoring (micro-motion sensing) as example applications to demonstrate the effectiveness of the proposed system. Extensive experiments show that SeRadar achieves highly accurate sensing even in challenging scenarios, significantly improving the robustness of mmWave sensing. To summarize, we made the following contributions in this paper.

- SeRadar is the first systematic framework to bring secondary reflections into the ecosystem of mmWave sensing. We show that the traditionally ignored secondary reflections can be utilized to address multiple well-known issues in mmWave sensing including blind spot, orientation-dependence and multi-target sensing.
- We address challenges including weak signal, path recognition, and multi-target interference to make sensing with secondary reflections work. We believe the proposed techniques can benefit other wideband signals such as UWB and ultrasound for sensing.
- We implemented the proposed system on commodity hardware and conducted comprehensive experiments to demonstrate the effectiveness of the proposed system. We show that secondary reflections can significantly increase the sensing accuracy and robustness, moving mmWave sensing one step towards real-life adoption.

2 PRELIMINARY

This section introduces the background knowledge of mmWave radar. mmWave radar operates in the 30-300 GHz frequency range. Frequency Modulated Continuous Wave (FMCW) is a commonly used modulation scheme for mmWave radar, which transmits periodic chirp signals with linearly increasing frequency over time. The transmitted signal can be represented as

$$S_{Tx}(t) = A_{Tx}\cos\left(2\pi\left(f_c t + \frac{B}{T_c}\frac{t^2}{2}\right)\right), \tag{1}$$

where A_{Tx} is the amplitude, f_c, B, and T_c are the starting frequency, bandwidth and chirp duration, respectively.

This mmWave signal is reflected by objects in the environment and captured at the receiver. After mixing and low-pass filtering, an intermediate frequency (IF) signal is generated. In complex environments, the received signal is the mix of multiple copies of the transmitted signal with varying delays and attenuation, corresponding to different paths which can

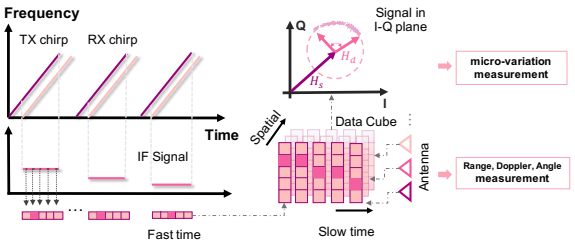

Figure 2: Signal processing procedures.

be represented as

$$S_{IF}(t) = \sum_{n=1}^{N} A_n \cos\left(2\pi\left(\frac{2BR_n}{cT_c}t - \frac{BR_n}{T_c}\right)\right), \tag{2}$$

where N represents the number of paths, A_n and R_n denote the amplitude and length of n-th path, and c is the speed of light. The received signal is processed across multiple dimensions: the fast-time dimension for a single chirp, the slow-time dimension across multiple chirps, and the spatial dimension for multiple transceiver pairs, as shown in Fig. 2.

Based on Eq. 2, it is evident that the IF frequency corresponding to a path length R_n is $f_{IF} = \frac{2BR_n}{cT_c}$. By performing an FFT operation, the peak frequency appears in the bin at f_{IF}, which enables distance estimation. When the target is in motion, it introduces a Doppler shift f_d on the signal. By extracting the phase variation, we can capture fine-grained motions with a displacement smaller than range resolution. The phase change between adjacent chirps can be used to estimate the Doppler velocity v_d as the time interval is known. In the spatial dimension, the angle of arrival (AoA) can be estimated by the phase difference of the signals received at different antennas. For adjacent antennas with a spacing of d_{int}, the phase difference (ϕ_{ant}) can be used to calculate AoA

$$\theta_n = \arcsin\left(\frac{\lambda\Delta\phi_{\text{ant}}}{2\pi d_{int}}\right). \tag{3}$$

3 MOTIVATION

3.1 Limitation of Primary Reflections

This section analyzes the limitations of traditional human sensing based on primary reflection, i.e., the signal is reflected only at the target and reaches the receiver without other intermediate reflections. However, primary reflections fail to work in multiple scenarios as illustrated in Fig. 1. (a) Primary reflection is occluded; (b) the target changes the orientation; and (c) strong interference exists among multiple targets close-by.

Without loss of generality, this section utilizes gesture recognition and respiration monitoring as application examples to illustrate the issues in relying only on primary reflections for sensing. As shown in Fig.3b, when the target is oriented towards the radar and is unobstructed, solutions based on primary reflections can accurately capture the gesture feature. However, when the target's orientation changes,

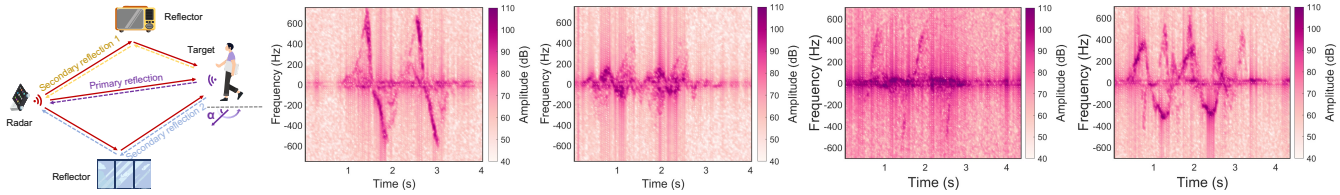

(a) Sensing settings. (b) Orientation: $\alpha = 0°$. (c) Orientation: $\alpha = 90°$. (d) Under Occlusion. (e) Under Interference.

Figure 3: Limitation of sensing via primary reflection.

Table 1: Degradation of breath monitoring reliability based on primary reflection

Case	Mean Absolute Error (bpm)
Ordinary condition	0.3
Orientation variation	4.7
Occlusion	5.1
Interference	8.6

gesture feature quality degrades as shown in Fig. 3c. When the primary reflection is occluded, the gesture feature can hardly be seen in Fig. 3d. When there are interferers near the target, the motion of the interferer is superimposed with the gesture of the target as shown in Fig. 3e.

We conducted benchmark experiments on respiration monitoring. Table 1 compares the mean absolute error in beat-per-minute (bpm) of primary reflection-based respiration monitoring in the three challenging scenarios with that under ordinary conditions. While the error is as low as 0.3 bpm under ordinary conditions, it increases to 4.7, 5.1, and 8.6 bpm in the challenging scenarios, much larger than the error requirement (below 1 bpm) for respiration sensing. The significant performance degradation highlights the limitations of primary reflection-based sensing.

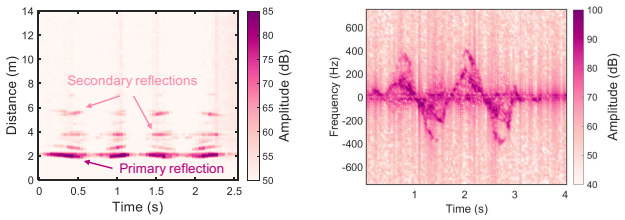

(a) Existence of multiple secondary reflections. (b) Features extracted via a secondary reflection ($\alpha = 90°$).

Figure 4: New opportunities via secondary reflections.

3.2 Opportunitiy via Secondary Reflections

In typical indoor settings, walls, ceilings, furniture, and appliances lead to rich secondary reflections. As shown in Fig. 4a, in addition to the primary reflection, multiple secondary reflections exist, which are caused by different reflectors in the environment. The secondary reflections are also sometimes called "ghosts". Interestingly, these secondary reflections can help when primary reflections suffer. As shown in Fig. 3a, when a reflector is in front of the target, this reflector leads to a secondary reflection path. Leveraging this secondary reflection, Fig. 4b shows a more reliable gesture pattern when the target orientation is at $\alpha = 90°$, compared to the pattern obtained in Fig. 3c. Similarly, for respiration sensing, using this secondary reflection, we can reduce the error from 4.7 bpm to 0.5 bpm. These results demonstrate the feasibility and capability of accurate sensing via secondary reflections.

4 THEORETICAL MODEL

4.1 Reflections via a Single Reflector

Fig. 5 illustrates different types of reflections. 1) **First-order primary reflection**: The mmWave signal gets reflected back directly from the target along the path $M \rightarrow T \rightarrow M$. 2) **Second-order secondary reflections**: There are two second-order reflection paths, $M \rightarrow R \rightarrow T \rightarrow M$ and $M \rightarrow T \rightarrow R \rightarrow M$, generating ghosts G_1 and G_2. 3) **Third-order secondary reflection**: This path involves two reflections, where the mmWave signal travels along path $M \rightarrow R \rightarrow T \rightarrow R \rightarrow M$, generating ghost G_3. We do not consider higher-order reflections because they are too weak to be utilized for sensing.

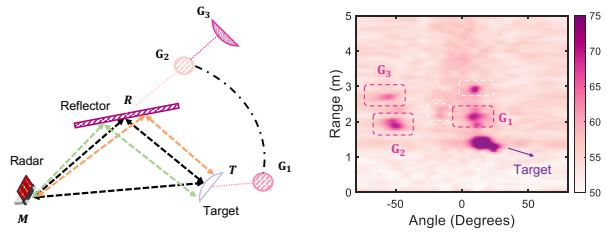

(a) Geometric model of secondary reflections. (b) Reflections reveal reflector and target directions.

Figure 5: The theoretical multi-reflection model.

4.2 Reflection via Multiple Reflectors

Besides the wall and ceiling, a lot of objects in the environment, such as home appliances and furniture, can also serve as the reflector. By extending our prior analysis of a single reflector to multiple reflectors, multiple secondary reflections can be generated. The rich secondary reflections help capture the target information from various angles, offering additional perspectives to enhance the sensing performance. As shown in Fig. 6a, reflector 1 and reflector 2 lead to secondary reflection #1 and #2, respectively, which contain

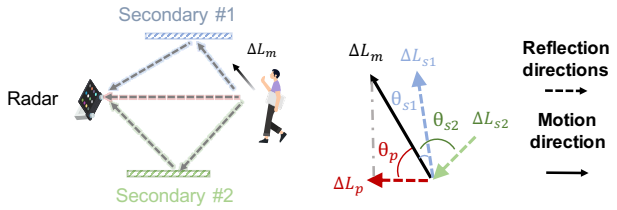

(a) Multi-view observation. (b) Correlated paths.

Figure 6: Reflectors provide multi-view observation.

target motion information from different angles that are complementary to that contained in the primary reflection. As shown in Fig. 6b, the target's hand motion with a displacement of ΔL_m can be decomposed into components along primary reflection's direction and the two secondary reflections' directions as ΔL_p, ΔL_{s1}, and ΔL_{s2}. The relationship between these displacement components can be expressed as $\frac{\Delta L_p}{\cos(\theta_p)} = \frac{\Delta L_{s1}}{\cos(\theta_{s1})} = \frac{\Delta L_{s2}}{-\cos(\theta_{s2})}$. This indicates a correlation exists between the motion components captured by primary reflection and secondary reflections.

5 SERADAR DESIGN

In this section, we first present an overview of SeRadar, followed by a detailed explanation of its components.

5.1 SeRadar Overview

Fig. 7 depicts the overview of SeRadar, which is composed of four modules: path enhancement, path selection, multi-user paths association, and path fusion.

- **Path Enhancement.** The secondary reflections are much weaker than primary reflection. Therefore, we propose to enhance the signal strength of secondary reflection via two schemes. Scheme 1: We first perform multi-directional beamforming to amplify all possible reflections. Scheme 2: We then identify similar signals reflected from different points of the same object and merge these reflections to further enhance signal strength.
- **Path Selection.** With lots of secondary reflections, we propose to select those that contain target information. Specifically, we select the secondary reflections that exhibit the target-induced signal variations. To quantify the signal variation, we employ a metric, Signal-Variation-to-Noise Ratio (SVNR).
- **Multi-user Paths Association.** In the multi-target scenario, it is challenging to match each secondary reflection to the corresponding target. We propose novel methods to categorize these secondary reflections and also associate them with their corresponding target. SeRadar further addresses the interference caused by multiple users, as their reflections can overlap and affect each other.
- **Path Fusion:** After identifying the effective secondary reflections, we fuse them to accurately extract human motion information, such as respiration rate estimation and gesture recognition. For micro motions, we implement direct path combination of secondary reflections, while for macro motions, we employ a multi-view sensing model to effectively combine the reflections from various directions.

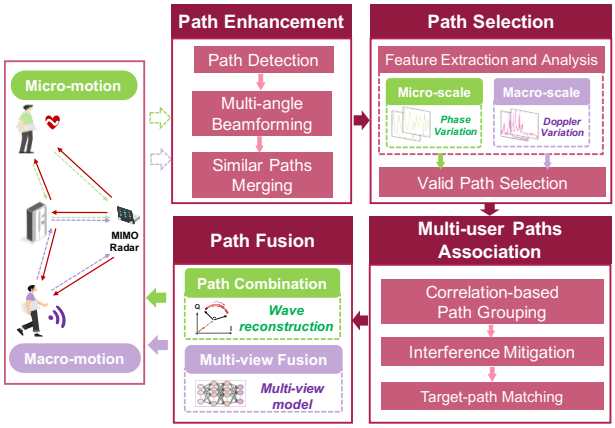

Figure 7: System overview of SeRadar.

5.2 Path Enhancement

Since secondary reflections are much weaker than primary reflections that are commonly used in traditional solutions, SeRadar proposes to enhance the signal strength of secondary reflections.

Path Detection. Before amplifying the reflections, SeRadar identifies the potential reflections (including primary and secondary reflections) without any knowledge of reflectors in the environment in advance. Specifically, SeRadar first generates the range-azimuth spectrum by calculating the Minimum Variance Distortionless Response (MVDR) [40] of the received signals. SeRadar then detects all the primary and secondary reflections from the range-azimuth spectrum, by applying the 2D Cell-Averaging Constant False Alarm Rate (CA-CFAR) algorithm. Since there are multiple reflections from the same object, these reflections are very close in the range and azimuth domains and form clusters in the range-azimuth spectrum. To accurately determine each reflection direction, we perform the DBSCAN clustering [42] and calculate the centroid of each cluster.

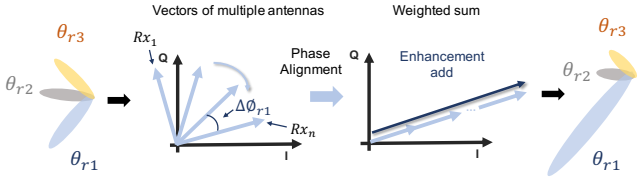

Figure 8: Example of beamforming at θ_{r1}.

Multi-angle Beamforming. We apply digital beamforming [17] to each azimuth angle to boost the strength of corresponding secondary reflections. After scanning across all azimuth angles, all the secondary reflections can be effectively enhanced. Specifically, for each direction, we align the phase values of signals received at multiple antennas.

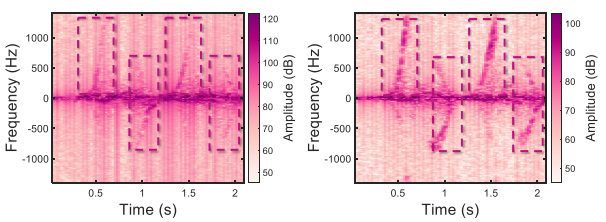

(a) Before path merging. **(b) After path merging.**

Figure 9: Time-frequency spectrums before and after merging similar signal paths from the same reflector.

The phase difference between two adjacent antennas can be calculated as $\Delta\phi_{ri} = \frac{2\pi}{\lambda} \cdot d_{int} \cdot \sin(\theta_{ri})$ where θ_{ri} represents the azimuth angle and d_{int} denotes the distance between two adjacent antennas. During phase alignment, SeRadar compensates the phase difference by applying $e^{-j(n-1)\Delta\phi_{ri}}$, where n denotes the antenna index. After the phase alignment, SeRadar adds the phase-aligned signals from each antenna constructively. The two steps described above can be modeled as follows

$$S_{BF_{\theta_{ri}}}(t) = \sum_{n=1}^{N} S_{IF,n}(t) \exp\left(-j(n-1)\Delta\phi_{ri}\right). \quad (4)$$

This beamforming process enhances the signal from the angle θ_{ri}, while the signals from other angles are randomly combined due to unaligned phase values. Fig. 8 shows an example of phase alignment at the azimuth angle of θ_{r1}.

Similar Paths Merging. As the size of the reflectors is usually much larger than the radar's range resolution, multiple signals can be reflected from different points on the same reflector, as shown in Fig. 5a, and they exhibit similar characteristics. SeRadar proposes to aggregate these reflections to further enhance the signal strength. Specifically, SeRadar first extracts the time-domain samples for each individual reflection signal. SeRadar then identifies the reflections from the same object by computing the correlation between their time-domain samples. Reflections with a correlation coefficient larger than a predefined threshold are considered to come from the same object. Note that these reflection signals share similar range bins, and the correlation is only performed for reflection signals whose range bin differences are smaller than l. After identifying these similar reflections, we add them up to enhance the signal strength. As shown in Fig. 9a, the secondary reflection signal before signal merging is very weak. In contrast, after merging similar reflection signals as presented in Fig. 9b, the signal strength is notably improved.

Here is the computational complexity analysis for the methods described. (1) Beamforming at N angles: $O(N \cdot T)$, where beamforming at each direction requires $O(T)$ operations. (2) Path correlation for m reflections with l adjacent bins: $O(m \cdot l \cdot T)$. Therefore, the overall complexity is $O(T \cdot (N + m \cdot l))$.

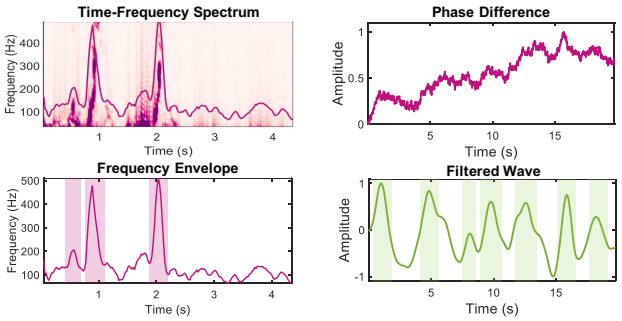

(a) Time-frequency spectrum and frequency envelope. **(b) Raw and filtered phase differences.**

Figure 10: Features extracted for (a) macro-motion and (b) micro-motion.

5.3 Path Selection

Although there are many secondary reflections in indoor environments, only some of them are reflected from the ROI of a target. To identify the "useful" reflections, SeRadar first extracts the signal variation for each reflection signal, analyzes the corresponding features, and then filters out those which exhibit little variation.

Feature Extraction and Analysis. For micro motion and macro motion, we extract the signal variation for each reflection path, but utilize different features. Specifically, for macro motion, such as gestures, its velocity causes a Doppler shift in the frequency domain. SeRadar leverages the Short-Time Fourier Transform (STFT) to obtain the time-frequency spectrogram and extracts the frequency envelope, as shown in Fig. 10a. For micro motion, such as respiration, the movement is much smaller than radar's range resolution (i.e., 4 cm), causing the frequency to remain stable over short periods and making the frequency envelope unavailable. As the phase value is sensitive to subtle movements, we extract the phase differences as the feature. We apply bandpass filters with specific frequency range (e.g., 0.2-1.5 Hz for respiration and 0.8-3 Hz for heart rate) to capture the micro motion of interest and then extract corresponding phase difference as presented in Fig. 10b.

Valid Path Selection. SeRadar introduces the Signal-Variation-to-Noise Ratio (SVNR) metric to quantify the quality of each reflection signal and selects those with high SVNR for sensing. The SVNR is defined as

$$SVNR = 10\log_{10}\left(\frac{P_{dynamic}}{P_{noise}}\right), \quad (5)$$

where $P_{dynamic}$ represents the power of signal feature variation, and P_{noise} denotes the noise power. For macro motion, the power of dynamic variation is calculated as $P_{dynamic} = \frac{1}{R_d}\sum_t \sum_{f\in\mathcal{F}_f} |S(t,f)|^2$, where $\mathcal{F}_f$ denotes the set of frequency components induced by the target motion, which are distributed around the frequency envelope in the time-frequency spectrum $S(t,f)$. Here, R_d is the number of elements in $\mathcal{F}_f$. The noise power, which is $P_{noise} = \frac{1}{R_n}\sum_t \sum_{f\notin\mathcal{F}_f} |S(t,f)|^2$,

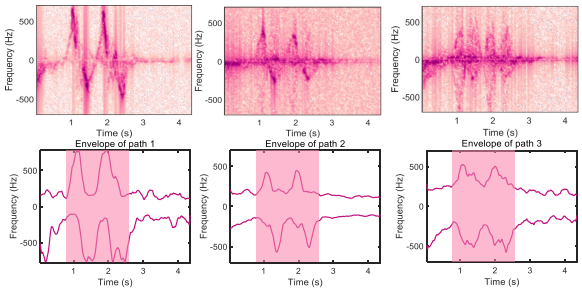

Figure 11: Examples of three paths within a correlation group, exhibiting synchronous variation.

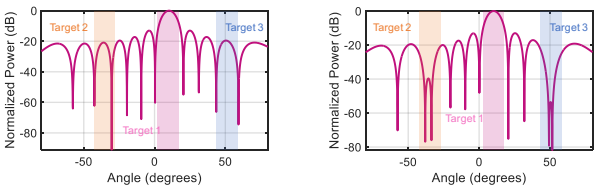

Figure 12: Beam pattern comparison of (a) before and (b) after null steering.

is calculated as the power of residual components after removing motion-induced components from time-frequency spectrogram, where R_n denotes the number of components after removing motion-induced components. To calculate the SVNR for micro motion, we perform FFT on the phase difference of each reflection signal to obtain the amplitude across all the frequency values, i.e., $\Phi_m(f)$. We then identify the frequency range of interest $[f_d, f_u]$ to mitigate the interference from other body motions. Specifically, we estimate the power in the frequency range $[f_d, f_u]$ as the dynamic power, i.e., $P_{dynamic} = \frac{1}{N_d}\sum_{f_d}^{f_u}|\Phi_m(f)|^2$. The power in the remaining frequencies is calculated as the noise power, i.e., $P_{noise} = \frac{1}{N_n}\sum_{f\notin[f_u,f_d]}|\Phi_m(f)|^2$. N_d and N_n represent the number of frequency values in $[f_d, f_u]$ and remaining frequency range, respectively. Finally, SeRadar sorts the SVNR values in descending order, and the top 70% of reflection signals, based on SVNR ranking, are selected, while the remaining 30% are discarded.

5.4 Multi-user Paths Association

After obtaining useful reflection signals, SeRadar proposes to associate them with the corresponding targets. To achieve this, SeRadar first categorizes these reflection signals by analyzing the correlation of their features. The reflections coming from the same target exhibit consistent characteristics, while the movements of different targets naturally differ in timing and patterns [71]. SeRadar further addresses the interference caused by multiple users, as their reflections can overlap and affect each other. Finally, we match the path group to the corresponding target.

Correlation-based Path Grouping. A single target motion (including both micro and macro motions) generates multiple reflections which are inherently correlated. Specifically, when the actual velocity of a human motion reaches its maximum, the velocity along each corresponding reflection path is also at its maximum. When the actual velocity of the gesture reaches its minimum, the velocity along each reflection path is also at its minimum. Therefore, for each target, the features (e.g., frequency envelope) of each reflection path exhibit peaks or valleys at similar timestamps, enabling us to exploit the correlation for reflection path grouping. Fig. 11 shows three secondary reflections for "push and pull" gesture performed twice. These three secondary reflections exhibit synchronous variations and belong to the same group. To identify reflections belonging to each target, SeRadar computes the correlations among these reflections and groups them based on their variation patterns. For macro motion, such as gesture, SeRadar applies correlations to the frequency envelopes of reflection paths. For micro motion, such as respiration, SeRadar applies correlation to the phase differences of reflection paths.

Specifically, SeRadar employs the Mutual Information Coefficient (MIC) as the metric [20] to calculate the correlations between each pair of paths, resulting in an $n \times n$ upper triangular matrix for n paths. Based on this matrix, SeRadar constructs an undirected graph $\mathbf{G}$, where each node represents a reflection signal, and edges are generated between paths whose MIC values are larger than the threshold τ. We then identify the groups based on the graph $\mathbf{G}$, where each group consists of connected nodes. The remaining paths are considered interference-affected or motion-irrelevant paths. Note that to avoid over-grouping, we adjust the number of path groups based on the number of targets. Specifically, if the number of detected groups exceeds the number of targets, we merge the groups with similar MIC values to ensure that the final number of path groups matches the target count.

Interference Mitigation. In multi-person scenarios, the reflections from different targets may overlap within the same range, resulting in interference. We observe that the primary reflections are more vulnerable to such interference, while secondary reflections are less likely to overlap. Additionally, when primary reflections of multiple targets overlap within the range bins, they are likely from different azimuths. Therefore, we extract each target's primary reflection by performing beamforming at the target direction and adopting null steering technique to suppress side lobe interference [29]. If there are multiple targets as shown in Fig. 12a, we first extract the reflection signal for one target (e.g., target 1), and null the side lobes towards other targets (e.g., target 2 and target 3) who are considered as interferers. We iteratively perform the same process until all the targets' reflections are extracted. To this end, we need to obtain a steering vector $\mathbf{w}_n$, which can (1) preserve the main lobe towards the target direction ϕ_t and (2) null the side lobe towards the interferers' directions ϕ_i. To meet the first requirement, the beamed pattern of $\mathbf{w}_n$, especially for the main lobe, is expected to be as similar as that of the steering vector

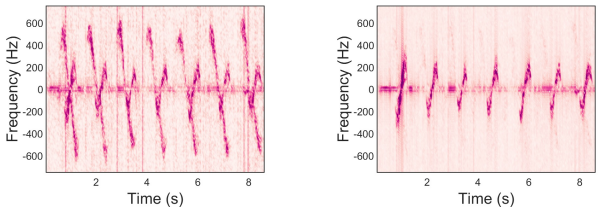

(a) Targets' features overlap. **(b) Feature for Target 1.**

Figure 13: The features (a) before and (b) after mitigating interference.

towards the target's direction, i.e., $\mathbf{w}_t$. Meanwhile, to satisfy the second requirement, $\mathbf{w}_n$ and the steering vector towards the interferers' directions, i.e., $\mathbf{w}_i$, should be orthogonal to each other. We formulate an optimization problem to null the side lobes as

$$\min \|\mathbf{w}_n - \mathbf{w}_t\|^2 \quad \text{s.t.} \quad \mathbf{w}_n^H \mathbf{C} = \mathbf{0}, \tag{6}$$

where $\mathbf{C} = \left[\mathbf{w}_{i1}, \mathbf{w}_{i2}, \ldots, \mathbf{w}_{ij}\right]$, and $\mathbf{w}_{ij}$ represents the steering vector of the j-th interferer' direction ϕ_{ij}, and $(\cdot)^H$ denotes the Hermitian transpose.

This optimization problem can be solved using the method of Lagrange multipliers to obtain the desired steering vector. After applying this method, as shown in Fig. 12b, target 2 at 37° and target 3 at 50° are suppressed. Fig. 13a and Fig. 13b demonstrate the frequency envelopes before and after applying our method. We can clearly see that the reflection signal of target 1 is more accurate after mitigating interference. Note that our method is implemented through quadratic optimization with linear constraints, and offers computational advantages over methods that involve more complex matrix operations and iterations [18].

Target-path Matching. Finally, SeRadar associates these reflection groups with their corresponding targets. Specifically, the primary reflections of targets can be utilized to estimate the targets' location relative to the mmWave radar, as well as the temporal characteristics of their motion. By leveraging spatiotemporal information, we can easily match each primary reflection to its corresponding target. Within each reflection group, the primary reflection serves as a key reference for target association. If the primary reflection is not available due to occlusion, SeRadar selects the most stable and strongest secondary reflection as an alternative.

5.5 Path Fusion

In this section, we explain how to leverage multiple reflection signals to extract the target motion information.

Path Combination for Micro-motion sensing. For micro motion, SeRadar combines correlated reflection signals to improve the subtle target-induced variations. As illustrated in Fig. 14a, these reflection paths exhibit stable and consistent variation patterns in the I/Q domain, which can be amplified. Our approach amplifies patterns through three

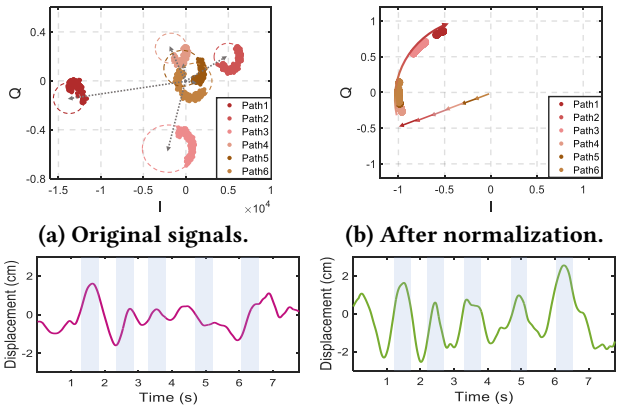

(a) Original signals. **(b) After normalization.**

(c) Sample of signal for a single reflection. **(d) Sample of signal for paths combination.**

Figure 14: Combination of multiple correlated paths.

specific steps: *1) Path Phase Alignment:* To effectively combine these reflection signals from different paths, SeRadar aligns their initial phases with the reference path's initial phase. The reference path typically is the primary reflection signal path. However, if the primary reflection is unavailable due to occlusion, SeRadar selects the strongest secondary reflection as the reference. Specifically, we adjust all the phase values of the reflection path by a constant to align its initial phase with that of the reference path. *2) Phase Normalization:* We then normalize phase changes of each reflection signal within a time window W, to ensure consistent phase change patterns. As shown in Fig. 14b, after phase normalization, all the reflection signals show synchronous and consistent variation. *3) Phase Weighting:* As the quality of reflection signals varies, we employ a voting-based weighting approach, which leverages SVNR and path correlation coefficient, to prioritize high-quality reflection signals. Specifically, the weight w_i for the i-th path is defined as

$$w_i = SVNR_i \cdot \text{Corr}\left[\phi_i(t), \bar{\phi}(t)\right] \tag{7}$$

where $SVNR_i$ represents the SVNR of the i-th reflection signal, $\phi_i(t)$ denotes the phase variation of the i-th reflection signal, and $\bar{\phi}(t)$ is the average phase variation of all the reflection signals within the path group. $\text{Corr}[\cdot,\cdot]$ calculates the correlation coefficient between two phase variations. Fig. 14c and 14d demonstrate the patterns before and after path combination for the scenario where target's chest is facing sideways to the radar. Before path combination, the target-induced signal variation is unstable, with larger fluctuations in some parts and smaller ones in others. After path combination, the variation becomes more stable.

Multi-view Fusion for Macro-motion Sensing. For macro motion, SeRadar proposes a deep learning-based multi-view model that leverages multiple reflection signals to recognize target motion, as shown in Fig. 15. Since the number of secondary reflections varies across different scenes, our approach aims to adapt to diverse scenes with an unknown

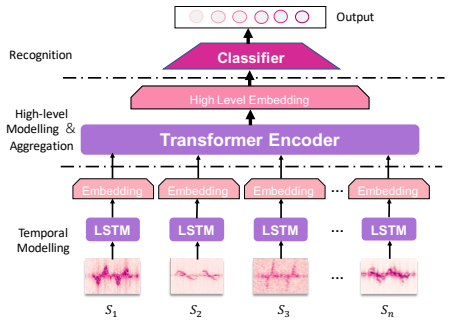

Figure 15: The architecture of multi-view model.

number of secondary reflections. Furthermore, each reflected signal is treated as a unique "view" for characterizing target motion, which is why our approach is referred to as a multi-view model. Our model comprises two main components: an LSTM module [15] for pre-encoding reflection paths to obtain temporal features, and a Transformer module [41] for extracting high-level features and aggregating reflection signals. We exclude the positional encodings in the Transformer model to achieve path permutation-invariant design, which allows flexible addition or removal of reflection signal paths. Specifically, suppose the input path data is $S = \{s^1, s^2, ..., s^n\}$ with an uncertain number of reflection signal paths. Our model is $M = M_{cls} \circ M_{trans} \circ M_{lstm}$, where M_{lstm}, M_{trans}, and M_{cls} are the LSTM encoder, Transformer aggregator, and linear classifier. Each path s^i is encoded by the LSTM as $enc_i = M_{lstm}(s^i)$ to get temporal feature embeddings of the target. The transformer aggregates them into a high-level embedding $agg_S = M_{trans}(\{enc_1, enc_2, ..., enc_n\})$, using self-attention to assign distinct attention weights to each path, capturing significant features and path dependencies. The final prediction is $y_S = M_{cls}(agg_S)$.

6 EVALUATION

6.1 Implementation and Setup

6.1.1 Implementation. We implement SeRadar on the TI AWR2944 EVM millimeter-wave radar module [1] that supports 4 Tx and 4 Rx antennas. In MIMO mode, it forms 12 horizontal equivalent antenna channels for high-resolution angle measurements (Fig. 16a). It operates in the frequency range of 76 to 81 GHz. Key parameters include a frame time of 40 ms, chirp duration of 312 μs, and a 160° Field of View (FOV). The AWR2944 EVM is connected to the DCA1000EVM data capture board to acquire raw intermediate frequency signals, which are then transmitted to a laptop via Ethernet [2]. Data processing is performed using MATLAB and Python. For ground truth, we use a piezoelectric respiratory belt and camera recordings.

6.1.2 Experimental setup. We deploy SeRadar in typical environments such as office, living room, vehicle cabin, and bedroom, as depicted in Fig. 16. Common objects, such as TVs, glass windows, ceilings, metal doors, and concrete walls are potential reflectors due to their high reflection coefficients and large size. Our experiments cover both single-person and multi-person settings. The radar is placed at fixed positions in various scenarios, while targets vary their positions and orientations relative to the radar, as shown in Fig. 16 and Fig. 19. We evaluate our system through micro-motion sensing (breathing monitoring) and macro-motion sensing (gesture recognition) tasks, which are widely adopted benchmarks in related work [4, 70]. We study multiple influencing factors, including target orientation changes, multi-person scenarios, LoS/NLoS scenarios, and target-reflector-radar distances. For all evaluations requiring model training, we collect the dataset with a 70:30 train-test split.

6.2 Overall Performance

6.2.1 Performance of macro-motion sensing. We evaluate SeRadar's performance for macro-motion sensing in five environments. During data collection, the target's position and posture vary as illustrated in Fig. 17b. The target performs gestures within a 5 m range from the radar with a distance d, orientation α, and azimuth β relative to the radar. β is incremented at a step size of 20° within the radar's effective FOV, and α is set at 0°, 45°, 90°, 180°, and 270°. Fig. 17a shows evaluated six common gestures: push (a), pull (b), arm circle (c), circle clockwise (d), lift (e), and wave (f). Note that the "secondary reflection" marked in Fig. 17c and subsequent figures represent the simultaneous use of both primary and secondary reflections. To evaluate the impact of target orientation, we build four datasets: Set 1 (orientation: 0° and 45°), Set 2 (orientation: 0°, 45° and 90°), Set 3 (orientation: 0°, 45°, 90° and 180°), and Set 4 (adding orientation of 270°). The model is trained on these orientation-specific sets and evaluated on a comprehensive dataset covering all the orientations.

Results demonstrate that target orientation significantly affects sensing performance, since different orientations produce distinct features (Fig. 3). Across various orientation sets, primary reflection-based methods achieve accuracy ranging from 63.16% to 74.03%. In contrast, with the help of secondary reflections, SeRadar enhances performance with accuracy from 80.10% to 92.43%. This highlights SeRadar's ability to utilize secondary reflections through multi-view analysis and maintain high accuracy even when primary reflection features are compromised. We further analyze the accuracy of individual gestures, as shown in Fig. 17d. For certain gestures, such as gestures a, b, and d, both primary and secondary reflection-based methods perform relatively well. However, for gestures c, e, and f, the performance using only primary reflection significantly declines to 64.28%, 71.43%, and 56.25%, while SeRadar still achieves a high accuracy above 90%. This improvement is due to the increased number of angles of view. Certain gestures exhibit similar features at specific angles, which cannot be distinguished by primary reflections, resulting in the degradation of performance.

(a) Hardware (b) Office (c) Living room (d) Vehicle cabin (e) Bedroom

Figure 16: Experiment settings.

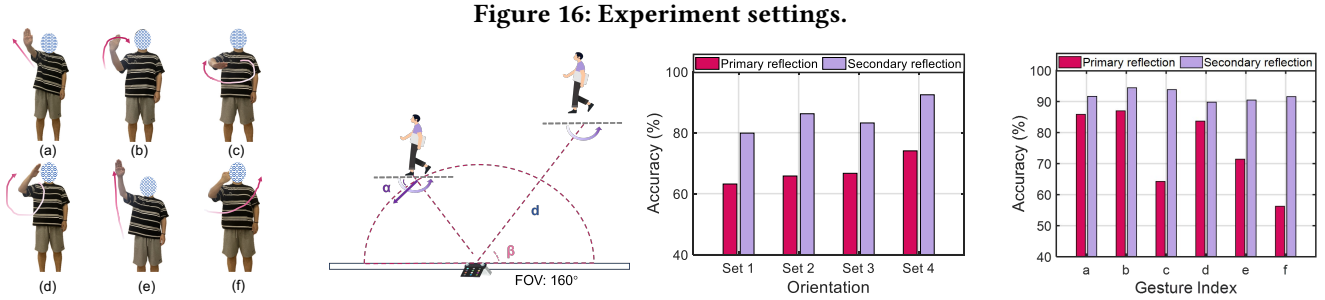

(a) Tested gestures. (b) Positions and orientations. (c) Different orientation. (d) Different gestures.

Figure 17: Experimental setting and performance of macro-motion sensing.

6.2.2 Performance of micro-motion sensing. This section evaluates the peformance of micro-motion sensing under orientation change and occlusion in indoor and vehicle cabin environments. Respiratory monitoring is based on the movement of the chest cavity, which varies with orientation due to posture changes. With the direction when the torso is facing the radar defined as 0°, we test the performance at 0°, 45°, 90°, and 180° for the indoor scenario and 0°, 45°, and 90° for the cabin scenario. We compare the average absolute respiratory rate error using primary reflection alone with the fusion of secondary reflections. Fig. 18 shows SeRadar's performance in indoor and cabin scenarios. Sensing based on the primary reflection shows large errors across all three orientations. The average absolute respiratory rate errors are 1.2 bpm, 5.4 bpm, and 7.1 bpm in the indoor scenario, while 3.5 bpm, 4.4 bpm, and 6.2 bpm in the cabin scenario. This is due to orientation changes, which make the observation of the chest's micro-movements less detectable through primary reflection. At the orientation of 0°, the primary reflection-based approach for respiration sensing achieves a small error of 0.2 bpm. In this case, incorporating the secondary reflection offers limited performance improvement. Moreover, seats and other obstacles in the cabin occlude the LoS path, even at 0°. In contrast, SeRadar yields a low respiration sensing error of 0.2 bpm, 0.3 bpm, and 0.5 bpm indoors, and 0.2 bpm, 0.5 bpm, and 0.7 bpm in the cabin, as it can identify secondary reflections exhibiting significant breathing patterns.

6.2.3 Comparison of path selection methods. We now compare SeRadar with two alternative path selection methods: (1) the optimal path approach based on idea of Trebsen [10] and (2) indiscriminate use of all secondary reflections. In the experiments, a single target performs either micro motion or

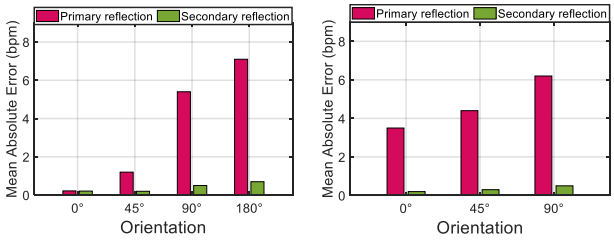

(a) In indoor scenarios. (b) In vehicle cabins.

Figure 18: Comparison for respiration sensing.

macro motion, while each motion is tested in four target orientations, i.e., 0°, 45°, 90°, and 180°. Moreover, the evaluation includes four different environments: a bedroom, a living room, an office and a vehicle cabin. The results are shown in Table 2. We observe that SeRadar outperforms the other two methods. This is because the optimal path approach lacks the motion information available in other secondary paths, and thus is not robust to the user's orientation change and environment change. Moreover, indiscriminate use of all secondary reflections introduces noise from irrelevant signals with low SVNR.

Table 2: Performance of path selection methods.

Method	Opt reflection	All reflections	SeRadar
Macro-motion	84.21%	87.57%	92.43%
Micro-motion	1.5 bpm	2.8 bpm	0.4 bpm

6.3 Performance in Multi-Person Scenarios

This section evaluates SeRadar's reliability in multi-person scenarios, where we test two to three users in motion at different locations. For micro-motion sensing, we examine respiration monitoring for rear-seat passengers who sit apart and sit together in the cabin, in addition to persons lying

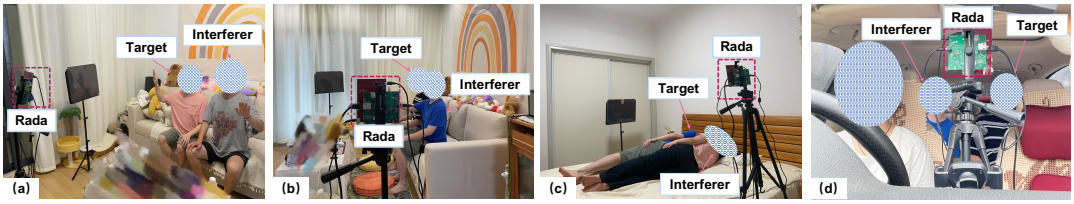

Figure 19: Experiment settings in multi-person scenarios. (a) and (b): sitting on the sofa; (c): lying on the bed; (d): sitting in the cabin.

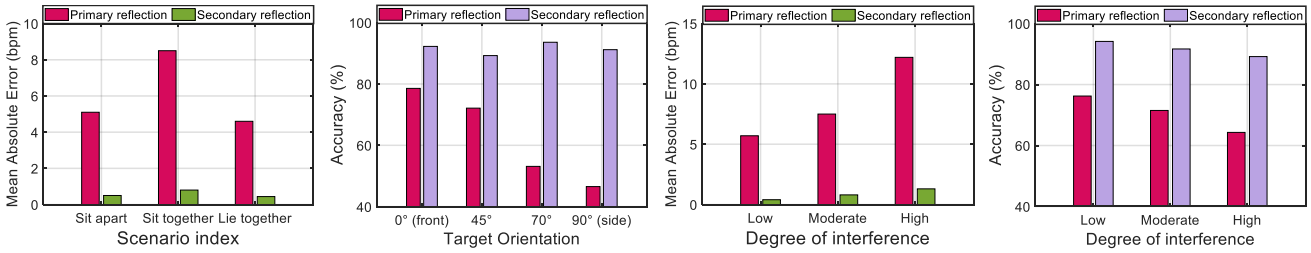

(a) Performance of respiration monitoring. **(b) Performance of gesture recognition.** **(c) Respiration monitoring performance under interference.** **(d) Gesture recognition performance under interference.**

Figure 20: Performance comparison in multi-person scenes.

close to each other in a bedroom, as shown in Fig.19 (d) and (c). For macro-motion sensing, we examine SeRadar's gesture recognition for targets who sit side by side on a sofa, where the target is interfered with or occluded by the adjacent person, as shown in Fig.19 (a) and (b). As shown in Fig. 20a, the errors based on primary reflections in three scenarios are 5.1 bpm, 8.5 bpm, and 4.6 bpm respectively while SeRadar's errors are 0.5 bpm, 0.8 bpm, and 0.44 bpm, which are significantly lower. This is because breathing signals overlap within the same range bin, leading to severe interference for primary reflections, while certain secondary reflections are less interfered with and more reliable. Fig. 20b illustrates the macro-motion sensing performance. The accuracy based on primary reflection under four settings ranges from 74.53% to 44.44%. This decline is attributed to the distortion and loss of primary reflection due to nearby movements or occlusions by other targets.

6.3.1 Impact of target's orientation. Meanwhile, we evaluate the impact of target's orientation. In this experiment, targets sit side by side, and their orientations vary from 0° (facing the radar) to 90° (side-facing). As shown in Fig. 20b, SeRadar maintains a gesture recognition accuracy above 89.25% across different orientations, demonstrating reliable sensing performance under varying target orientations.

6.3.2 Performance under varying levels of interference. We further conduct experiments to investigate SeRadar's reliability under varying degrees of interference. For micro-motion sensing, interference is categorized as follows: slight chest movements (Low), pronounced chest movements (Moderate), and additional torso movements (High). For macro-motion sensing, interference is classified as slight hand movements (Low), slight torso movements (Moderate), and combined torso and hand movements (High). As shown in Fig. 20c and Fig. 20d, both mean absolute error (MAE) and accuracy using primary reflections suffer with an increasing level of interference. In contrast, SeRadar still maintains reliable performance with small performance degradation under increasing interference, with an MAE of 0.83 bpm for micro sensing and an accuracy of 91.67% for macro sensing. These experiments demonstrate the reliability improvement of SeRadar by leveraging secondary reflections.

6.3.3 Impact of distance between targets. In this experiment, we reduce the distance between two targets from 2 m to 0.2 m to evaluate SeRadar's resolution. Both targets perform gestures simultaneously toward the radar: one with large, rapid, and variable movement, while the other with subtle and slow motion. The results are shown in Fig. 21. When the distance between targets becomes smaller than 0.3 m, SeRadar's average accuracy for the large and subtle movements decreases slightly to 89.12% and 81.67%, respectively. This demonstrates SeRadar's reliable performance with multiple persons in relatively close proximity.

6.4 Impact of Different Factors

6.4.1 Impact of environment type. This experiment evaluates the performance in two bedrooms (BR1 and BR2), a living room (LR), a dining room (DR), and an office (OFF). These environments vary in size, structure, and positions of environmental reflectors. Take gesture recognition as an example, Fig. 23a shows the recognition accuracy across different environments with the highest accuracy occurs in two bedrooms (94%) while the accuracy in the office and living room is lower (88%). Such performance gap stems from the average path SVNR difference, which is shown in Fig. 23b. The bedrooms are smaller in size with a higher concentration of reflectors, resulting in a larger SVNR due to reduced path

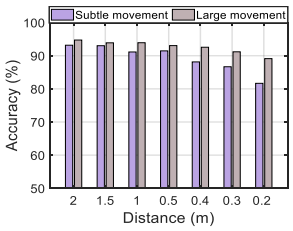

Figure 21: Impact of distance between targets.

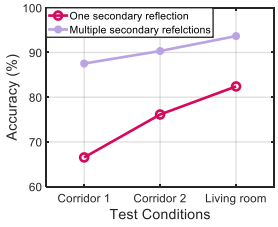

Figure 22: Performance for out-of-view targets.

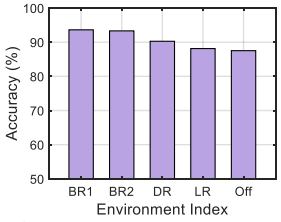

(a) Gesture recognition.

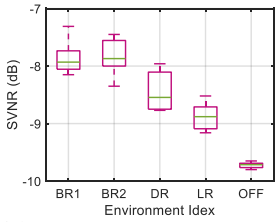

(b) SVNR in five scenarios.

Figure 23: The impact of environments.

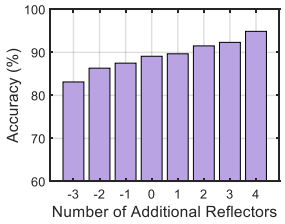

(a) Impact of number.

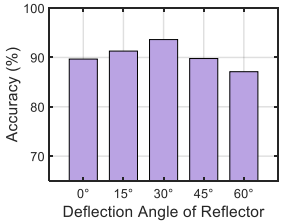

(b) Impact of orientation.

Figure 24: The impact of reflectors.

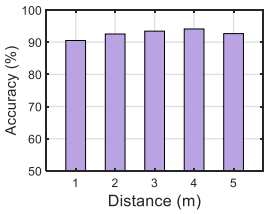

(a) Gesture recognition.

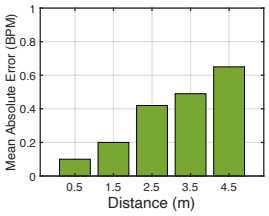

(b) Respiration monitoring.

Figure 25: Impact of distance from reflector and target.

loss. In contrast, in a larger and more spacious environment, such as the office, the SVNR deteriorates due to decreased signal quality and fewer effective paths. The results indicate that sensing with secondary reflections performs better in smaller spaces with a higher density of reflectors.

6.4.2 Performance for out-of-view target. This section assesses SeRadar's performance when the target is out of the mmWave radar's field of view, which means primary reflection can not be detected via mmWave radar. The evaluation covers two corridors (marked as Corridor 1 and Corridor 2) and a living room with a cabinet obstructing the target. Fig. 22 compares the performance that using the strongest secondary reflection with those obtained by utilizing all useful secondary reflections. Specifically, leveraging all secondary reflections achieves at least 10% higher performance compared to relying solely on the strongest secondary reflection, demonstrating the need of path fusion. Note that primary reflection solutions are ineffective for out-of-view targets since no primary reflections are available.

6.4.3 Impact of reflector quantity. Now we evaluate the impact of reflector quantity. We conduct experiments in a living room with natural reflectors, such as TV and glass window, and vary the number of reflectors by removing or adding specific objects. To reduce the number of reflectors, we remove large existing objects (e.g., TV and glass windows). To increase the number of reflectors, we deploy 1~4 additional metal plates. Note that we do not retrain our sensing model when varying the number of reflectors. Fig. 24a presents the experiment results. The sensing performance of SeRadar improves as the number of reflectors increases. Specifically, in the original environment without adding or removing objects, SeRadar achieves a gesture recognition accuracy of 89.10%. With 4 additional reflectors, the accuracy increases to 94.89%, while the accuracy reduces to 83.13% with 3 reflectors removed. This demonstrates that sensing performance is higher with more reflectors, while ordinary environment objects (e.g., walls and furniture) can enable SeRadar to maintain good performance and reliability.

6.4.4 Impact of the reflector orientation. We further evaluate the impact of reflector orientation. Without loss of generality, we employ TV, a large natural reflector, as the representative reflector. In our setup, 0° indicates that the TV is perpendicular to the radar's center line. We gradually rotate the TV from 0° to 60° relative to its original position. Our sensing model is not retrained when the orientation varies. As shown in Fig. 24b, the sensing performance varies with the orientation of reflector, because the change of reflector orientation can alter the corresponding secondary path, which in turn affects the performance. Specifically, the accuracy of gesture recognition is the largest (93.62%) at the orientation of 30°, and gradually degrades at other angles.

6.4.5 Impact of distance from target and reflectors. The distance between the reflector, the target, and the radar affects signal propagation and feature quality. First, we vary the target-reflector distance from 0.5 m (1 m) to 4.5 m (5 m) for micro (Macro) motion sensing, while fixing the distance between the radar and reflector. As shown in Fig. 25, breathing error remains below 0.7 bpm, while gesture recognition is minimally affected, maintaining accuracy above 90.5%. We then vary the target-radar distance from 0.5 m (1 m) to 4.5 m (5 m) for micro (Macro) motion sensing, while fixing the distance between the target and reflector. Similar results are achieved, with gesture recognition accuracy maintained above 91.21% and breathing rate error kept below 0.8 bpm.

7 DISCUSSION

Sensing Limitations. (1) The quality of secondary reflections depends on the environment and reflectors (size, amount, and materials). For example, secondary reflections can be significantly attenuated in case of absorptive materials (thick carpets or acoustic foam). In open environments with fewer reflectors, the number of effective secondary reflections decreases, leading to smaller performance gains. On the other hand, in such open scenarios, the likelihood of primary reflections being blocked or encountering interference is also reduced. (2) The proposed correlation grouping method works well for simple motion, e.g., push and pull. However, it is challenging to group the secondary reflections for complex motions (e.g., vigorous dancing) which exhibit intricate patterns over space and time. We believe a potential solution is to leverage deep learning to enhance the grouping of secondary reflections for complex motions.

Sensing for Mobile Targets. Target mobility introduces additional interference. The signal variation from the region of interest (e.g., the chest for respiration or the hands for gestures) becomes mixed with signal variations from other body parts, leading to sensing failures. Prior works [4, 9] have explored this challenging issue, primarily focusing on primary reflections. These methods can be extended to enable sensing via secondary reflections for mobile targets. For example, by analyzing reflections from different body regions, motion artifacts caused by other body movements and device displacement can be identified and eliminated [4].

8 RELATED WORK

mmWave-based Sensing. mmWave radar leverages the short wavelength, wide bandwidth, and multi-element antenna array to achieve fine-grained tracking resolution. These benefits facilitate the widespread adoption of mmWave radars in everyday sensing tasks, such as gesture recognition [31, 33, 48], human activity monitoring [6, 34, 65], vital signs monitoring [4, 14, 56], material identification [36], speech recognition [27, 44], blood pressure monitoring [37], and facial recognition [54, 67]. Despite their great success, the reliance on primary reflections poses significant challenges for real-world deployment, as primary reflections can be occluded, affected by sensing angles, and disrupted by interference from other targets.

Recent works tackle this issue through additional deployments, either by introducing extra mmWave radars to increase the number of primary reflections [22, 30] or by leveraging metasurfaces to modify primary reflections [32, 49]. While effective, these solutions introduce additional hardware costs and increase deployment complexity. GWaltz [16] utilizes the observation of coherent multipath reflections to complement one-dimensional view of the radar, enabling two-dimensional trajectory tracking of the rotor. Trebsen [10] optimizes both the transmitter radar and receiver radar's waveform to identify a better sensing direction other than the primary reflection. However, our extensive analysis shows that typical settings contain multiple secondary reflections, which can be combined effectively. SeRadar aims to provide a comprehensive sensing solution using secondary reflections, without requiring prior knowledge of the reflectors or environmental settings.

Sensing with Other Wireless technologies. In addition to mmWave-based sensing, researchers have explored the use of other wireless technologies for sensing, including WiFi [23, 60], Bluetooth [11], LoRa [5, 51], and UWB [62, 63]. Among them, WiFi-based solutions are particularly promising due to WiFi's widespread coverage. Similarly, these wireless sensing systems often suffer from performance degradation in complex environments, particularly under non-line-of-sight (NLOS) conditions [39]. As a remedy, recent works have explored the use of metasurfaces to enhance sensing reliability [12] or leverage ambient reflected signals in NLoS environments [26]. Despite the advantages of secondary reflections, it is challenging for WiFi sensing systems to adopt the proposed strategy because the limited bandwidth is insufficient to separate secondary reflections from the primary ones. Bluetooth and LoRa sensing systems face similar challenges. Beyond WiFi, UWB-based solutions are also popular due to UWB's low power consumption and cost-effective hardware. It is worth noting that SeRadar's design principle of leveraging secondary reflections could be extended to UWB, given its large bandwidth.

Wireless Localization. Prior research works have explored the use of multiple reflections for localization and tracking [58, 64]. For instance, iLocScan [61] models the indoor multipath propagation and leverages the geometric relationship between the device and reflection points for simultaneous localization and floor plan reconstruction. However, localization and sensing are dramatically different tasks, and secondary reflections have not yet been exploited in mmWave sensing. In this work, we introduce secondary reflections into the ecosystem of mmWave human sensing for the first time.

9 CONCLUSION

This paper introduces SeRadar, a novel mmWave sensing framework that systematically exploits secondary reflections—commonly overlooked in wireless sensing—to tackle critical challenges in real-world sensing applications. Extensive experiments conducted in diverse settings demonstrate that SeRadar significantly improves reliability. We believe this framework advances mmWave sensing towards real-life adoption and can also benefit sensing applications using other wideband signals.

ACKNOWLEDGMENTS

This research is partially supported by ECS CityU 21216822, City University of Hong Kong 9610491, NSFC under Grant 62272098, NTU SUG-NAP, GRF CityU 11216324, and JC STEM Lab of Smart City (Ref.: 2023-0108).

REFERENCES

[1] Awr2944evm. https://www.ti.com/tool/AWR2944EVM. Accessed: 2024.

[2] Dca1000evm. https://www.ti.com/tool/DCA1000EVM. Accessed: 2024.

[3] Cai, C., Pu, H., Wang, P., Chen, Z., and Luo, J. We hear your pace: Passive acoustic localization of multiple walking persons. *Proc. ACM Interact. Mob. Wearable Ubiquitous Technol. 5*, 2 (jun 2021).

[4] Chang, Z., Zhang, F., Xiong, J., Chen, W., and Zhang, D. Msense: Boosting wireless sensing capability under motion interference. In *Proceedings of the 30th Annual International Conference on Mobile Computing and Networking* (2024), pp. 108–123.

[5] Chang, Z., Zhang, F., Xiong, J., Ma, J., Jin, B., and Zhang, D. Sensor-free soil moisture sensing using lora signals. *Proc. ACM Interact. Mob. Wearable Ubiquitous Technol. 6*, 2 (jul 2022).

[6] Chen, A., Wang, X., Zhu, S., Li, Y., Chen, J., and Ye, Q. mmbody benchmark: 3d body reconstruction dataset and analysis for millimeter wave radar. In *Proceedings of the 30th ACM International Conference on Multimedia* (2022), pp. 3501–3510.

[7] Chen, L., Xiong, J., Chen, X., Lee, S. I., Zhang, D., Yan, T., and Fang, D. Lungtrack: Towards contactless and zero dead-zone respiration monitoring with commodity rfids. *Proc. ACM Interact. Mob. Wearable Ubiquitous Technol. 3*, 3 (sep 2019).

[8] Chen, Z., Yang, P., Xiong, J., Feng, Y., and Li, X.-Y. Tagray: Contactless sensing and tracking of mobile objects using cots rfid devices. In *IEEE INFOCOM 2020 - IEEE Conference on Computer Communications* (2020), pp. 307–316.

[9] Chen, Z., Zheng, T., Cai, C., and Luo, J. MoVi-Fi: motion-robust vital signs waveform recovery via deep interpreted RF sensing. In *Proceedings of the 27th Annual International Conference on Mobile Computing and Networking* (New Orleans Louisiana, Oct. 2021), ACM, pp. 392–405.

[10] Fan, L., Xie, L., Zhou, W., Wang, C., Bu, Y., and Lu, S. Beamforming for sensing: Hybrid beamforming based on transmitter-receiver collaboration for millimeter-wave sensing. *Proceedings of the ACM on Interactive, Mobile, Wearable and Ubiquitous Technologies 8*, 2 (2024), 1–27.

[11] Fan, X., Li, G., Lin, Z., Hu, Y., Liu, Y., Jiang, T., Yin, Z., Qian, F., Wang, S., and Chan, S.-H. G. Experiences of deploying a citywide crowdsourcing platform to search for missing people with dementia. In *Proceedings of the 30th Annual International Conference on Mobile Computing and Networking* (New York, NY, USA, 2024), ACM MobiCom '24, Association for Computing Machinery, p. 200–214.

[12] Feng, C., Li, X., Zhang, Y., Wang, X., Chang, L., Wang, F., Zhang, X., and Chen, X. Rflens: metasurface-enabled beamforming for iot communication and sensing. In *Proceedings of the 27th Annual International Conference on Mobile Computing and Networking* (2021), pp. 587–600.

[13] Gong, J., Zhang, X., Lin, K., Ren, J., Zhang, Y., and Qiu, W. RF Vital Sign Sensing under Free Body Movement. *Proceedings of the ACM on Interactive, Mobile, Wearable and Ubiquitous Technologies 5*, 3 (Sept. 2021), 1–22.

[14] Gong, J., Zhang, X., Lin, K., Ren, J., Zhang, Y., and Qiu, W. Rf vital sign sensing under free body movement. *Proceedings of the ACM on Interactive, Mobile, Wearable and Ubiquitous Technologies 5*, 3 (2021), 1–22.

[15] Greff, K., Srivastava, R. K., Koutník, J., Steunebrink, B. R., and Schmidhuber, J. Lstm: A search space odyssey. *IEEE transactions on neural networks and learning systems 28*, 10 (2016), 2222–2232.

[16] Guo, J., Jin, M., He, Y., Wang, W., and Liu, Y. Dancing Waltz with Ghosts: Measuring Sub-mm-Level 2D Rotor Orbit with a Single mmWave Radar. In *Proceedings of the 20th International Conference on Information Processing in Sensor Networks (co-located with CPS-IoT Week 2021)* (Nashville TN USA, May 2021), ACM, pp. 77–92.

[17] Ha, U., Assana, S., and Adib, F. Contactless seismocardiography via deep learning radars. In *Proceedings of the 26th annual international conference on mobile computing and networking* (2020), pp. 1–14.

[18] Hadad, E., Doclo, S., and Gannot, S. The binaural lcmv beamformer and its performance analysis. *IEEE/ACM Transactions on Audio, Speech, and Language Processing 24*, 3 (2016), 543–558.

[19] Jiang, H., Zhang, J., Guo, X., and He, Y. Sense Me on the Ride: Accurate Mobile Sensing over a LoRa Backscatter Channel. In *Proceedings of the 19th ACM Conference on Embedded Networked Sensor Systems* (Coimbra Portugal, Nov. 2021), ACM, pp. 125–137.

[20] Kinney, J. B., and Atwal, G. S. Equitability, mutual information, and the maximal information coefficient. *Proceedings of the National Academy of Sciences 111*, 9 (2014), 3354–3359.

[21] Kong, H., Xu, X., Yu, J., Chen, Q., Ma, C., Chen, Y., Chen, Y.-C., and Kong, L. m3track: mmwave-based multi-user 3d posture tracking. In *Proceedings of the 20th Annual International Conference on Mobile Systems, Applications and Services* (2022), pp. 491–503.

[22] Li, S., Guo, J., Xi, R., Duan, C., Zhai, Z., and He, Y. Pedestrian trajectory based calibration for multi-radar network. In *IEEE INFOCOM 2021-IEEE Conference on Computer Communications Workshops (INFOCOM WKSHPS)* (2021), IEEE, pp. 1–2.

[23] Li, X., Wang, H., Chen, Z., Jiang, Z., and Luo, J. Uwb-fi: Pushing wi-fi towards ultra-wideband for fine-granularity sensing. In *Proceedings of the 22nd Annual International Conference on Mobile Systems, Applications and Services* (New York, NY, USA, 2024), MOBISYS '24, Association for Computing Machinery, p. 42–55.

[24] Liu, H., Cui, K., Hu, K., Wang, Y., Zhou, A., Liu, L., and Ma, H. mTransSee: Enabling Environment-Independent mmWave Sensing Based Gesture Recognition via Transfer Learning. *Proceedings of the ACM on Interactive, Mobile, Wearable and Ubiquitous Technologies 6*, 1 (Mar. 2022), 1–28.

[25] Liu, J., Liu, H., Chen, Y., Wang, Y., and Wang, C. Wireless Sensing for Human Activity: A Survey. *IEEE Communications Surveys & Tutorials 22*, 3 (2020), 1629–1645.

[26] Liu, J., Zeng, Y., Gu, T., Wang, L., and Zhang, D. WiPhone: Smartphone-based Respiration Monitoring Using Ambient Reflected WiFi Signals. *Proceedings of the ACM on Interactive, Mobile, Wearable and Ubiquitous Technologies 5*, 1 (Mar. 2021), 1–19.

[27] Liu, T., Gao, M., Lin, F., Wang, C., Ba, Z., Han, J., Xu, W., and Ren, K. Wavoice: A noise-resistant multi-modal speech recognition system fusing mmwave and audio signals. In *Proceedings of the 19th ACM Conference on Embedded Networked Sensor Systems* (2021), pp. 97–110.

[28] Liu, Y., Yu, A., Wang, L., Guo, B., Li, Y., Yi, E., and Zhang, D. Unifi: A unified framework for generalizable gesture recognition with wi-fi signals using consistency-guided multi-view networks. *Proc. ACM Interact. Mob. Wearable Ubiquitous Technol. 7*, 4 (jan 2024).

[29] Madani, S., Jog, S., Lacruz, J. O., Widmer, J., and Hassanieh, H. Practical null steering in millimeter wave networks. In *18th USENIX Symposium on Networked Systems Design and Implementation (NSDI 21)* (2021), pp. 903–921.

[30] Meng, Z., Fu, S., Yan, J., Liang, H., Zhou, A., Zhu, S., Ma, H., Liu, J., and Yang, N. Gait recognition for co-existing multiple people using millimeter wave sensing. In *Proceedings of the AAAI Conference on Artificial Intelligence* (2020), vol. 34, pp. 849–856.

[31] Palipana, S., Salami, D., Leiva, L. A., and Sigg, S. Pantomime: Mid-air gesture recognition with sparse millimeter-wave radar point clouds. *Proceedings of the ACM on interactive, mobile, wearable and ubiquitous technologies 5*, 1 (2021), 1–27.

[32] Qian, K., Yao, L., Zhang, X., and Ng, T. N. Millimirror: 3d printed reflecting surface for millimeter-wave coverage expansion. In *Proceedings of the 28th Annual International Conference on Mobile Computing And Networking* (New York, NY, USA, 2022), MobiCom '22, Association

for Computing Machinery, p. 15–28.

[33] Santhalingam, P. S., Hosain, A. A., Zhang, D., Pathak, P., Rangwala, H., and Kushalnagar, R. mmasl: Environment-independent asl gesture recognition using 60 ghz millimeter-wave signals. *Proceedings of the ACM on Interactive, Mobile, Wearable and Ubiquitous Technologies 4*, 1 (2020), 1–30.

[34] Sen, A., Das, A., Pradhan, S., and Chakraborty, S. Continuous multi-user activity tracking via room-scale mmwave sensing. In *2024 23rd ACM/IEEE International Conference on Information Processing in Sensor Networks (IPSN)* (2024), IEEE, pp. 163–175.

[35] Shanbhag, H., Madani, S., Isanaka, A., Nair, D., Gupta, S., and Hassanieh, H. Contactless Material Identification with Millimeter Wave Vibrometry. In *Proceedings of the 21st Annual International Conference on Mobile Systems, Applications and Services* (Helsinki Finland, June 2023), ACM, pp. 475–488.

[36] Shanbhag, H., Madani, S., Isanaka, A., Nair, D., Gupta, S., and Hassanieh, H. Contactless material identification with millimeter wave vibrometry. In *Proceedings of the 21st Annual International Conference on Mobile Systems, Applications and Services* (New York, NY, USA, 2023), MobiSys '23, Association for Computing Machinery, p. 475–488.

[37] Shi, Z., Gu, T., Zhang, Y., and Zhang, X. mmbp: Contact-free millimetre-wave radar based approach to blood pressure measurement. In *Proceedings of the 20th ACM Conference on Embedded Networked Sensor Systems* (2022), pp. 667–681.

[38] Shuai, X., Shen, Y., Tang, Y., Shi, S., Ji, L., and Xing, G. milliEye: A Lightweight mmWave Radar and Camera Fusion System for Robust Object Detection. In *Proceedings of the International Conference on Internet-of-Things Design and Implementation* (Charlottesvle VA USA, May 2021), ACM, pp. 145–157.

[39] Sun, Y., He, Y., Zhang, J., Na, X., Chen, Y., Wang, W., and Guo, X. Bifrost: Reinventing wifi signals based on dispersion effect for accurate indoor localization. SenSys '23, Association for Computing Machinery, p. 376–389.

[40] Tzafri, L., and Weiss, A. J. High-resolution direct position determination using mvdr. *IEEE Transactions on Wireless Communications 15*, 9 (2016), 6449–6461.

[41] Vaswani, A., Shazeer, N., Parmar, N., Uszkoreit, J., Jones, L., Gomez, A. N., Kaiser, Ł., and Polosukhin, I. Attention is all you need. *Advances in neural information processing systems 30* (2017).

[42] Wagner, T., Feger, R., and Stelzer, A. Modification of dbscan and application to range/doppler/doa measurements for pedestrian recognition with an automotive radar system. In *2015 European Radar Conference (EuRAD)* (2015), IEEE, pp. 269–272.

[43] Wang, C., Lin, F., Liu, T., Zheng, K., Wang, Z., Li, Z., Huang, M.-C., Xu, W., and Ren, K. mmEve: eavesdropping on smartphone's earpiece via COTS mmWave device. In *Proceedings of the 28th Annual International Conference on Mobile Computing And Networking* (Sydney NSW Australia, Oct. 2022), ACM, pp. 338–351.

[44] Wang, C., Lin, F., Liu, T., Zheng, K., Wang, Z., Li, Z., Huang, M.-C., Xu, W., and Ren, K. mmeve: eavesdropping on smartphone's earpiece via cots mmwave device. In *Proceedings of the 28th Annual International Conference on Mobile Computing And Networking* (New York, NY, USA, 2022), MobiCom '22, Association for Computing Machinery, p. 338–351.

[45] Wang, J., Xiong, J., Chen, X., Jiang, H., Balan, R. K., and Fang, D. Tagscan: Simultaneous target imaging and material identification with commodity rfid devices. In *Proceedings of the 23rd Annual International Conference on Mobile Computing and Networking* (New York, NY, USA, 2017), MobiCom '17, Association for Computing Machinery, p. 288–300.

[46] Wang, K., Shi, C., Cheng, J., Wang, Y., Xie, M., and Chen, Y. Solving the wifi sensing dilemma in reality leveraging conformal prediction. In *Proceedings of the 20th ACM Conference on Embedded Networked Sensor Systems* (New York, NY, USA, 2023), SenSys '22, Association for Computing Machinery, p. 407–420.

[47] Wang, Z., Ren, Y., Chen, Y., and Yang, J. Toothsonic: Earable authentication via acoustic toothprint. *Proc. ACM Interact. Mob. Wearable Ubiquitous Technol. 6*, 2 (jul 2022).

[48] Wei, H., Li, Z., Galvan, A. D., Su, Z., Zhang, X., Pahlavan, K., and Solovey, E. T. Indexpen: Two-finger text input with millimeter-wave radar. *Proceedings of the ACM on Interactive, Mobile, Wearable and Ubiquitous Technologies 6*, 2 (2022), 1–39.

[49] Woodford, T., Qian, K., and Zhang, X. Metasight: High-resolution nlos radar with efficient metasurface encoding. In *Proceedings of the 21st ACM Conference on Embedded Networked Sensor Systems* (2023), pp. 308–321.

[50] Wu, C., Zhang, F., Wang, B., and Liu, K. R. msense: Towards mobile material sensing with a single millimeter-wave radio. *Proceedings of the ACM on Interactive, Mobile, Wearable and Ubiquitous Technologies 4*, 3 (2020), 1–20.

[51] Xie, B., Cui, M., Ganesan, D., Chen, X., and Xiong, J. Boosting the Long Range Sensing Potential of LoRa. In *Proceedings of the 21st Annual International Conference on Mobile Systems, Applications and Services* (Helsinki Finland, June 2023), ACM, pp. 177–190.

[52] Xie, B., Cui, M., Ganesan, D., and Xiong, J. Wall matters: Rethinking the effect of wall for wireless sensing. *Proc. ACM Interact. Mob. Wearable Ubiquitous Technol. 7*, 4 (jan 2024).

[53] Xie, D., Wang, X., and Tang, A. MetaSight: localizing blocked RFID objects by modulating NLOS signals via metasurfaces. In *Proceedings of the 20th Annual International Conference on Mobile Systems, Applications and Services* (Portland Oregon, June 2022), ACM, pp. 504–516.

[54] Xie, J., Kong, H., Yu, J., Chen, Y., Kong, L., Zhu, Y., and Tang, F. mm3dface: Nonintrusive 3d facial reconstruction leveraging mmwave signals. In *Proceedings of the 21st Annual International Conference on Mobile Systems, Applications and Services* (2023), pp. 462–474.

[55] Xu, C., Li, H., Li, Z., Zhang, H., Rathore, A. S., Chen, X., Wang, K., Huang, M.-c., and Xu, W. CardiacWave: A mmWave-based Scheme of Non-Contact and High-Definition Heart Activity Computing. *Proceedings of the ACM on Interactive, Mobile, Wearable and Ubiquitous Technologies 5*, 3 (Sept. 2021), 1–26.

[56] Xu, C., Li, H., Li, Z., Zhang, H., Rathore, A. S., Chen, X., Wang, K., Huang, M.-c., and Xu, W. Cardiacwave: A mmwave-based scheme of non-contact and high-definition heart activity computing. *Proc. ACM Interact. Mob. Wearable Ubiquitous Technol. 5*, 3 (sep 2021).

[57] Xu, W., Song, W., Liu, J., Liu, Y., Cui, X., Zheng, Y., Han, J., Wang, X., and Ren, K. Mask does not matter: anti-spoofing face authentication using mmWave without on-site registration. In *Proceedings of the 28th Annual International Conference on Mobile Computing And Networking* (Sydney NSW Australia, Oct. 2022), ACM, pp. 310–323.

[58] Xu, X., Meng, X., Tong, X., Liu, X., Xie, X., and Qu, W. Hypertracking: Exploring the hyperbolic model for non-line-of-sight device-free wi-fi tracking. *Proceedings of the ACM on Interactive, Mobile, Wearable and Ubiquitous Technologies 7*, 4 (2024), 1–26.

[59] Yi, E., Wu, D., Xiong, J., Zhang, F., Niu, K., Li, W., and Zhang, D. BFMSense: WiFi sensing using beamforming feedback matrix. In *21st USENIX Symposium on Networked Systems Design and Implementation (NSDI 24)* (Santa Clara, CA, Apr. 2024), USENIX Association, pp. 1697–1712.

[60] Zeng, Y., Wu, D., Xiong, J., Liu, J., Liu, Z., and Zhang, D. Multisense: Enabling multi-person respiration sensing with commodity wifi. *Proc. ACM Interact. Mob. Wearable Ubiquitous Technol. 4*, 3 (sep 2020).

[61] Zhang, C., Li, F., Luo, J., and He, Y. ilocscan: Harnessing multipath for simultaneous indoor source localization and space scanning. In *Proceedings of the 12th ACM Conference on Embedded Network Sensor*

Systems (2014), pp. 91–104.

[62] Zhang, F., Chang, Z., Xiong, J., Ma, J., Ni, J., Zhang, W., Jin, B., and Zhang, D. Embracing consumer-level uwb-equipped devices for fine-grained wireless sensing. *Proc. ACM Interact. Mob. Wearable Ubiquitous Technol. 6*, 4 (jan 2023).

[63] Zhang, F., Xiong, J., Chang, Z., Ma, J., and Zhang, D. Mobi2sense: empowering wireless sensing with mobility. In *Proceedings of the 28th Annual International Conference on Mobile Computing And Networking* (New York, NY, USA, 2022), MobiCom '22, Association for Computing Machinery, p. 268–281.

[64] Zhang, X., Chen, L., Feng, M., and Jiang, T. Toward Reliable Non-Line-of-Sight Localization Using Multipath Reflections. *Proceedings of the ACM on Interactive, Mobile, Wearable and Ubiquitous Technologies 6*, 1 (Mar. 2022), 1–25.

[65] Zhang, X., Li, Z., and Zhang, J. Synthesized millimeter-waves for human motion sensing. In *Proceedings of the 20th ACM Conference on Embedded Networked Sensor Systems* (2022), pp. 377–390.

[66] Zhang, X., Zhang, Y., Shi, Z., and Gu, T. mmFER: Millimetre-wave Radar based Facial Expression Recognition for Multimedia IoT Applications. In *Proceedings of the 29th Annual International Conference on Mobile Computing and Networking* (Madrid Spain, Oct. 2023), ACM, pp. 1–15.

[67] Zhang, X., Zhang, Y., Shi, Z., and Gu, T. mmfer: Millimetre-wave radar based facial expression recognition for multimedia iot applications. In *Proceedings of the 29th Annual International Conference on Mobile Computing and Networking* (2023), pp. 1–15.

[68] Zhang, Y., Hou, W., Yang, Z., and Wu, C. VeCare: Statistical acoustic sensing for automotive In-Cabin monitoring. In *20th USENIX Symposium on Networked Systems Design and Implementation (NSDI 23)* (Boston, MA, Apr. 2023), USENIX Association, pp. 1185–1200.

[69] Zhao, P., Lu, C. X., Wang, J., Chen, C., Wang, W., Trigoni, N., and Markham, A. mid: Tracking and identifying people with millimeter wave radar. In *2019 15th International Conference on Distributed Computing in Sensor Systems (DCOSS)* (2019), IEEE, pp. 33–40.

[70] Zheng, K., Qian, K., Woodford, T., and Zhang, X. Neuroradar: A neuromorphic radar sensor for low-power iot systems. In *Proceedings of the 21st ACM Conference on Embedded Networked Sensor Systems* (New York, NY, USA, 2024), SenSys '23, Association for Computing Machinery, p. 223–236.

[71] Zheng, T., Chen, Z., Zhang, S., and Luo, J. Catch your breath: Simultaneous rf tracking and respiration monitoring with radar pairs. *IEEE Transactions on Mobile Computing 22*, 11 (2022), 6283–6296.

[72] Zheng, Y., Zhang, Y., Qian, K., Zhang, G., Liu, Y., Wu, C., and Yang, Z. Zero-effort cross-domain gesture recognition with wi-fi. In *Proceedings of the 17th Annual International Conference on Mobile Systems, Applications, and Services* (New York, NY, USA, 2019), MobiSys '19, Association for Computing Machinery, p. 313–325.

[73] Zhu, G., Hu, Y., Wang, B., Wu, C., Gao, W., and Liu, K. J. R. Demo: Practical wifi sensing for human and non-human motion identification on the edge. MOBISYS '24, Association for Computing Machinery, p. 608–609.